J|A|C|S
ARTICLES

Published on Web 08/09/2008

Control of Vertex Geometry, Structure Dimensionality, Functionality, and Pore Metrics in the Reticular Synthesis of Crystalline Metal−Organic Frameworks and Polyhedra

Hiroyasu Furukawa,*,† Jaheon Kim,‡ Nathan W. Ockwig,§ Michael O'Keeffe,|| and Omar M. Yaghi*,†

Department of Chemistry and Biochemistry, Center for Reticular Chemistry at the California NanoSystems Institute, University of California, Los Angeles, California 90095-1569, Department of Chemistry, Soongsil University, Seoul 156-743, Korea, Geochemistry Department, Sandia National Laboratories, Albuquerque, New Mexico 87185-0754, and Department of Chemistry and Biochemistry, Arizona State University, Tempe, Arizona 85287-1604

Received May 27, 2008; E-mail: furukawa@chem.ucla.edu; yaghi@chem.ucla.edu

Abstract: Metal−organic polyhedra and frameworks (MOPs and MOFs) were prepared by linking square units $M_2(CO_2)_4$ (M = Cu and Zn) with a variety of organic linkers designed to control the dimensionality (periodicity) and topology of the resulting structures. We describe the preparation, characterization, and crystal structures of 5 new MOPs and 11 new MOFs (termed MOP-14, -15, -17, -23, -24 and MOF-114, -115, -116, -117, -118, -119, -222, -601, -602, -603, -604) and show how their structures are related to the shape and functionality of the building blocks. The gas uptake behaviors of MOP-23 and MOF-601 to -603 are also presented as evidence that these structures have permanent porosity and rigid architectures.

Introduction

Paddlewheel Structures with One Kind of Linker. The newly emerging field of reticular chemistry is concerned with linking of building blocks known as secondary building units (SBUs) into predetermined structures using strong bonds.[1] It has been applied particularly to the synthesis of porous metal−organic polyhedra (MOPs) and frameworks (MOFs).[2] One can now reproducibly prepare many SBUs of different shapes, and one of the remaining major challenges lies in designing links that will produce the desired topology while simultaneously allowing control of metrics and functionality of the pores.

In an earlier contribution[3] we described the major ways in which square SBUs can be linked by one kind of linker to form polyhedra or extended structures with periodicity in one, two, or three dimensions. Some of these were realized using the $Cu_2(-CO_2)_4$ "paddlewheel" SBU and using dicarboxylic acid linkers with shapes expressly designed to produce the target product and which were the simplest possible to guarantee the desired result. However, quite often linkers of the same general shape but of different lengths are used to produce an *isoreticular* (same topology) series of compounds,[4] although sometimes a serendipitous variant of the designed topology is discovered.[5] In this contribution we have more extensively explored the degree to which synthesis involving linked paddlewheels can be directed toward a targeted topology using more complex functionalized linkers with less ideal shapes and less rigidity.

We first indicate how periodicity ("dimensionality") is controlled by linker shape. We note (see Figure 1A) that the points of extension of the paddlewheel unit, the four C atoms, form a square, and we may abstract this SBU by a square. We start from the simplest, and historically first, case:[6] in Figure 1A we show two paddlewheels linked by 1,4-benzenedicarboxylate. The $-CO_2$ (carboxylate) groups are coplanar, and the squares of the SBU are related by simple translations. Continuation of this structure with the same link produces the 2-periodic planar structure.

† University of California, Los Angeles.
‡ Soongsil University.
§ Sandia National Laboratories.
|| Arizona State University.

(1) Yaghi, O. M.; O'Keeffe, M.; Ockwig, N. W.; Chae, H. K.; Eddaoudi, M.; Kim, J. *Nature* **2003**, *423*, 705–714.
(2) (a) Kitagawa, S.; Kitaura, R.; Noro, S. *Angew. Chem., Int. Ed.* **2004**, *43*, 2334–2375. (b) Tranchemontagne, D. J.; Ni, Z.; O'Keeffe, M.; Yaghi, O. M. *Angew. Chem., Int. Ed.* **2008**, *47*, 5136–5147. (c) Papaefstathiou, G. S.; MacGillivray, L. R. *Angew. Chem., Int. Ed.* **2002**, *41*, 2070–2073. (d) Chun, H.; Dybtsev, D. N.; Kim, H.; Kim, K. *Chem.—Eur. J.* **2005**, *11*, 3521–3529. (e) Ma, B.-Q.; Mulfort, K. L.; Hupp, J. T. *Inorg. Chem.* **2005**, *44*, 4912–4914. (f) Shimizu, G. K. H. *J. Solid State Chem.* **2005**, *178*, 2519–2526. (g) Halper, S. R.; Do, L.; Stork, J. R.; Cohen, S. M. *J. Am. Chem. Soc.* **2006**, *128*, 15255–15268. (h) Lee, J. Y.; Olson, D. H.; Pan, L.; Emge, T. J.; Li, J. *Adv. Funct. Mater.* **2007**, *17*, 1255–1262. (i) Feller, R. K.; Forster, P. M.; Wudl, F.; Cheetham, A. K. *Inorg. Chem.* **2007**, *46*, 8717–8721. (j) Ma, S.; Sun, D.; Ambrogio, M.; Fillinger, J. A.; Parkin, S.; Zhou, H.-C. *J. Am. Chem. Soc.* **2007**, *129*, 1858–1859.
(3) Eddaoudi, M.; Kim, J.; Vodak, D.; Sudik, A.; Wachter, J.; O'Keeffe, M.; Yaghi, O. M. *Proc. Natl. Acad. Sci. U.S.A.* **2002**, *99*, 4900–4904.
(4) (a) Chae, H. K.; Kim, J.; Delgado-Friedrichs, O.; O'Keeffe, M.; Yaghi, O. M. *Angew. Chem., Int. Ed.* **2003**, *42*, 3907–3909. (b) Eddaoudi, M.; Kim, J.; Rosi, N.; Vodak, D.; Wachter, J.; O'Keeffe, M.; Yaghi, O. M. *Science* **2002**, *295*, 469–472. (c) Surblé, S.; Serre, C.; Mellot-Draznieks, C.; Millange, F. G.; Férey, G. *Chem. Commun.* **2006**, 284–286.
(5) (a) Chae, H. K.; Siberio-Pérez, D. Y.; Kim, J.; Go, Y.-B.; Eddaoudi, M.; Matzger, A. J.; O'Keeffe, M.; Yaghi, O. M. *Nature* **2004**, *427*, 523–527. (b) Devic, T.; David, O.; Valls, M.; Marrot, J.; Couty, F.; Férey, G. *J. Am. Chem. Soc.* **2007**, *129*, 12614–12615.
(6) Li, H.; Eddaoudi, M.; Groy, T. L.; Yaghi, O. M. *J. Am. Chem. Soc.* **1998**, *120*, 8571–8572.

 10.1021/ja803783c CCC: $40.75

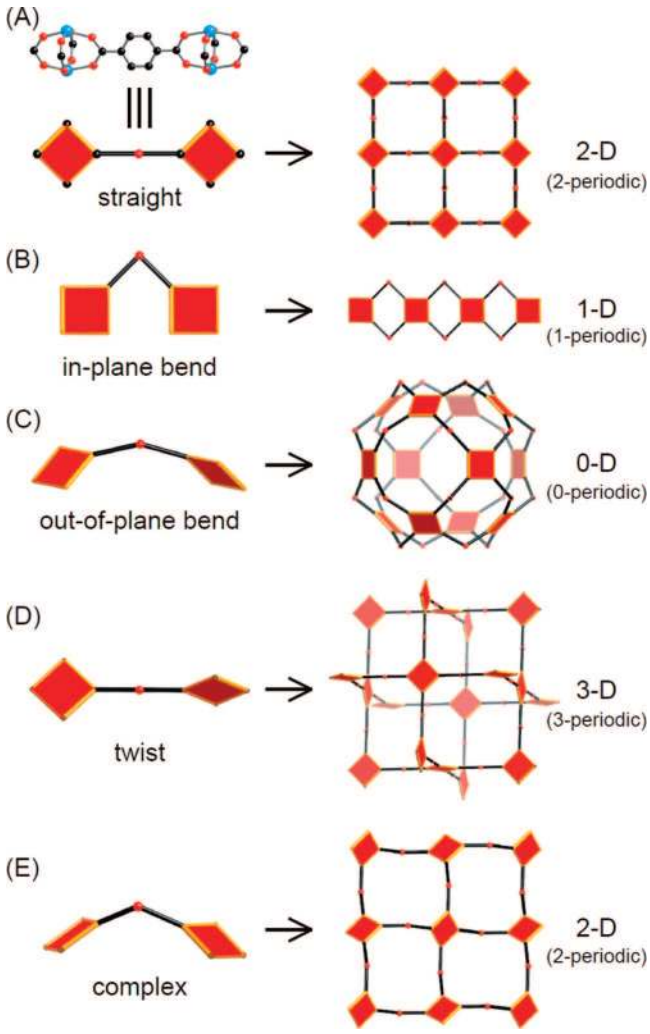

Figure 1. Schematic representation of ditopic organic links connected between two square paddlewheels (left). The corresponding default structures (right) expected to result from syntheses employing organic links with the appropriate angles between two squares.

Now we consider linkers distorted from this basic shape. If the linker is bent in the plane of the original, it will lead to linear rods of linked paddlewheels as shown in Figure 1B; we display two examples of this case below.

Alternatively bending the linkers out of the plane will result in paddlewheels which are not coplanar on a curved surface. With this, the suitable angle of bend will produce a finite (0-periodic) polyhedral molecule. A 90° bend will lead to a molecule with six paddlewheels arranged as the square faces of a truncated polyhedron.[7] Moreover, a 120° bend will produce a polyhedral structure formed from 12 paddlewheels as shown schematically in Figure 1C. Several examples of this geometry have already been reported.[8] Here we exhibit five more structures with new functional groups on the surface of the polyhedra.

The final distortion we consider is a 90° twist that leads to a 3-periodic structure with the topology of the 3-periodic net, **nbo** (Figure 1D).[9,10]

We note that the simultaneous presence of several distortion modes can lead to less predictable results. For a wide range of unsymmetric linker geometries it is possible to produce a corrugated layer as shown in Figure 1E. Such layers have been observed,[11] and we show another example in this work.

Structures with Two Linker Geometries. The structures of Figure 1 have just one kind of link. The general problem of enumerating geometries of structures with more than one kind of link is very complex and beyond the scope of this paper. However in our earlier work[3] we noted an example (MOF-112) in which there were straight links, some with twist and some without and here we pose the question of what structures there are of this sort (mixed links) with just one kind of vertex. In such structures, along an edge the orientations of the connected squares will either be the same (S) or twisted (T). In cyclic order around a vertex the possibilities are SSSS, SSST, SSTT, STST, STTT, and TTTT. Based on experiments with model building, we believe that an extended structure with only STTT vertices is not possible and that the others lead to unique structures which are shown in Figure 2.[12]

STST corresponds to the common **cds** net,[9] which we encounter below. As far as we know, the others with both S and T links have not yet been made as MOFs and remain an interesting synthetic challenge. The net of MOF-112 has STST and TTTT vertices in the ratio 2:1.

The *edge nets* derived from these nets by placing vertices in the middle of each edge (and removing the original vertices) are of interest. Vertices in an S edge have square coordination, and vertices in a T edge have tetrahedral coordination. The edge net of TTTT (**nbo**) is the sodalite net (**sod**). The edge net of STST (**cds**) is **pts** which has just one kind of link and two kinds of vertex and is the most symmetrical way of linking square and tetrahedral vertices. The edge net of SSST has three kinds of vertex and again the minimum number (two) of linking edges and could be an interesting target for synthesis.

In this contribution we describe the synthesis and structure of 5 new MOPs and 11 new MOFs (termed MOP-14, -15, -17, -23, -24 and MOF-114, -115, -116, -117, -118, -119, -222, -601, -602, -603, -604), which illustrate the construction principles described above. We further show how their structures are related to the shape and functionality of the organic building

(7) Ni, Z.; Yassar, A.; Antoun, T.; Yaghi, O. M. *J. Am. Chem. Soc.* **2005**, *127*, 12752–12753.

(8) (a) Eddaoudi, M.; Kim, J.; Wachter, J. B.; Chae, H. K.; O'Keeffe, M.; Yaghi, O. M. *J. Am. Chem. Soc.* **2001**, *123*, 4368–4369. (b) Furukawa, H.; Kim, J.; Plass, K. E.; Yaghi, O. M. *J. Am. Chem. Soc.* **2006**, *128*, 8398–8399. (c) Moulton, B.; Lu, J.; Mondal, A.; Zaworotko, M. J. *Chem. Commun.* **2001**, 863–864. (d) Abourahma, H.; Coleman, A. W.; Moulton, B.; Rather, B.; Shahgaldian, P.; Zaworotko, M. J. *Chem. Commun.* **2001**, 2380–2381. (e) McManus, G. J.; Wang, Z.; Zaworotko, M. J. *Cryst. Growth Des.* **2004**, *4*, 11–13. (f) Ke, Y.; Collins, D. J.; Zhou, H.-C. *Inorg. Chem.* **2005**, *44*, 4154–4156.

(9) We use the symbols (bold) of the RCSR database (www.rcsr.anu.edu.au) net as shown on Figure 2.

(10) Eddaoudi, M.; Kim, J.; O'Keeffe, M.; Yaghi, O. M. *J. Am. Chem. Soc.* **2002**, *124*, 376–377.

(11) (a) Abourahma, H.; Bodwell, G. J.; Lu, J.; Moulton, B.; Pottie, I. R.; Walsh, R. B.; Zaworotko, M. J. *Cryst. Growth Des.* **2003**, *3*, 513–519. (b) Bourne, S. A.; Lu, J.; Mondal, A.; Moulton, B.; Zaworotko, M. J. *Angew. Chem., Int. Ed.* **2001**, *40*, 2111–2113.

(12) If we do not restrict to a 90° twist, the number of possibilities is vast. Also, two uninodal ones we know with pure twist (no bend) are **qzd** and **qdl** (60° twist).[9] Although these occur, a way of designing a linker with a twist not equal to 90° remains to be found. Moreover, nets like **rhr**[9] have complicated combinations of twist and bend angles that differ from 90° and are even further from *designed* synthesis. Therefore, we focused our study upon the 0° straight (S) and 90° twist (T). Bends and twists of other angles are topics of a different paper.

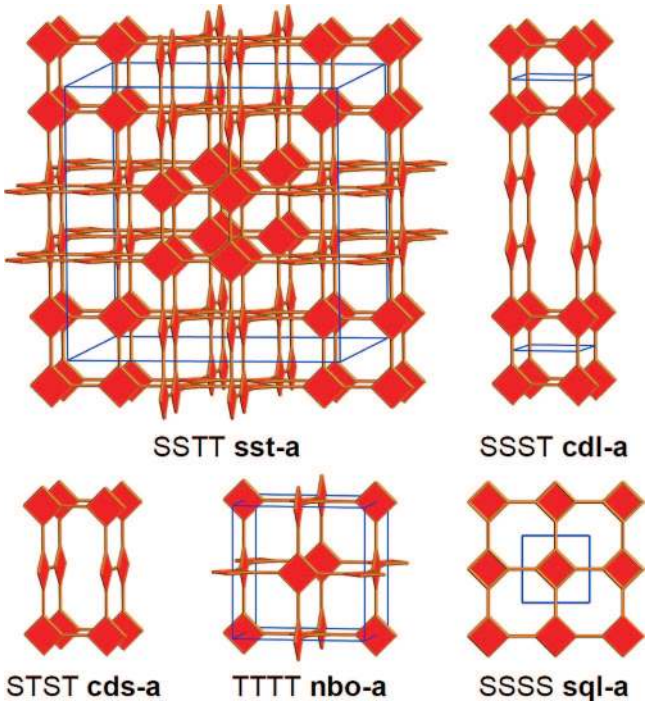

Figure 2. Structures comprised of square units which have the same environment but for which adjacent squares can be either in the same plane (S) or twisted at 90° (T). A symbol such as **nbo-a** indicates that the original **nbo** net has been *augmented*; in this case each of the original vertices is replaced by a square of vertices.

blocks. Gas uptake measurements are reported for MOP-23 and MOF-601 to -603 to show that these structures have permanent porosity.

Experimental Section

Linkers Used in This Work. Figure 3 illustrates the ditopic organic linkers used in this study. They were obtained as follows: 5-Bromo-1,3-benzenedicarboxylic acid ($H_2$5-Br-*m*BDC), 5-amino-1,3-benzenedicarboxylic acid ($H_2$5-NH_2-*m*BDC), and biphenyl-4,4′-dicarboxylic acid (H_2BPDC) were purchased from Aldrich Chemical Co., and 4,4′-dicarboxydiphenyl sulfone (H_2DCPS) and benzophenone-4,4′-dicarboxylic acid (H_2KDB) were purchased from TCI America. These chemicals were used without further purification. 2,7-Biphenylenedicarboxylic acid ($H_2$2,7-BPDC),[13] 5-allyloxobenzene-1,3-dicarboxylic acid ($H_2$5-allyloxo-*m*BDC),[14] and 4,4′-azodibenzoate (H_2ADB)[15] were prepared according to published procedures.

Dimethyl-2,7-naphthalenedicarboxylate (TCI America) was hydrolyzed to obtain 2,7-naphthalenedicarboxylic acid ($H_2$2,7-NDC). Dimethyl-2,2′-diiodo-4,4′-biphenyldicarboxylate was prepared according to published procedures and hydrolyzed to obtain a corresponding acid (H_2IBPDC).[13b] The dicyano compound (2,2′-dicyano-4,4′-biphenyldicarboxylic acid, H_2CNBPDC) was prepared as follows:[16] a mixture of dimethyl-2,2′-diiodo-4,4′-biphenyldicarboxylate and CuCN in dry 1-methyl-2-pyrrolidinone (NMP) was refluxed for 6 h. After cooling, the mixture was poured into a mixture of $FeCl_3 \cdot 6H_2O$ and conc. HCl/water (1:6, v/v). The resulting mixture was stirred at 60 °C for 20 min, extracted with dichloromethane, and hydrolyzed with 1 M sodium hydroxide/ethanol (1:4, v/v) at room temperature for 12 h. Dimethyl-2,2′-dimethyl-4,4′-dicalboxylate and 4,4′-dicyano-3,3′-dimethylbiphenyl were synthesized via Ni(0)-catalyzed polymerization of methyl 4-bromo-3-methylbenzoate (Aldrich) and 4-bromo-2-methylbenzonitrile (Acros)[17] and hydrolyzed to obtain 2,2′-dimethyl-4,4′-biphenlydicarboxylic acid ($H_2$2-MeBPDC) and 3,3′-dimethyl-4,4′-biphenyldicarboxylic acid ($H_2$3-MeBPDC). Friedel−Crafts acylation of 1,1′-binaphthyl synthesized from 1-bromonaphthalene (Aldrich)[17] was performed according to published procedures and oxidized to obtain 1,1′-binaphthyl-4,4′-dicarboxylic acid (H_2BNDC).[18] 4,4′-((1*S*,2*S*)-1,2-Dimethoxyethane-1,2-diyl)dibenzoic acid (H_2*S*,*S*-DMEDBA) was kindly obtained from Prof. N. Jeong (Korea University).

Analytical Techniques. Single crystal X-ray diffraction data were collected on a Bruker SMART APEX CCD-based X-ray diffractometer equipped with a normal focus Mo-target X-ray tube ($\lambda = 0.710\ 73$ Å). Powder X-ray diffraction (PXRD) patterns were obtained with a Bruker D8 Advance diffractometer (monochromated Cu Kα ($\lambda = 1.540\ 56$ Å) radiation). The simulated powder patterns were calculated from the single crystal X-ray diffraction data and generated with PowderCell 2.3.[19] FT-IR spectra were measured from KBr pellets using a Nicolet FT-IR 400 system. Thermal gravimetric analysis (TGA) was performed using a TA Q500 thermal analysis system at a heating rate of 5 °C min^{-1} under a dry nitrogen flow. Elemental microanalyses (EA) were performed by The University of Michigan Department of Chemistry using a Perkin-Elmer CHN 2400 Series II thermal analysis system.

Low pressure gas adsorption isotherms were measured volumetrically on an Autosorb-1 analyzer (Quantachrome Instruments).[20] A liquid nitrogen sample bath (77 K) was used for N_2 and H_2, while ice water (273 K) was used for the CO_2 isotherm measurements. The N_2, Ar, H_2, and CO_2 gases used were UHP grade. For measurement of the apparent surface areas (S_{Lang}), the Langmuir method was applied using the adsorption branches of the N_2 isotherms assuming a N_2 cross-sectional area of 16.2 $Å^2$/molecule. The pore size distribution and the cumulative pore volumes were calculated from the isotherm data. The micropore volumes (V_p) were determined using the Dubinin−Raduskavich (DR) transformed N_2 isotherms across the linear region of the low pressure data.

Synthesis and Characterization of MOPs and MOFs. For easy reference, the formulas for 5 MOPs and 11 MOFs, and their crystal unit cell parameters are listed in Tables 1 (MOPs) and 2 (MOFs). All metal salts and solvents (DMF = *N*,*N*-dimethylformamide, NMP = 1-methyl-2-pyrrolidinone, EtOH = ethanol, Py = pyridine, DMA = *N*,*N*-dimethylacetamide, THF = tetrahydrofuran) except for *N*,*N*-diethylformamide (DEF, BASF) were purchased from Fisher Chemicals and used without further purification.

Cu_{24}(5-Br-*m*BDC)$_{24}$(DMF)$_8$(Gly-*t*Bu)$_8$(H_2O)$_8$·(DMF)$_{32}$(H_2O)$_{20}$, MOP-14. Glycine *tert*-butyl ester hydrochloride (Gly-*t*Bu·HCl, 242 mg, Aldrich) was dissolved in 6.0 mL of DMF and triethylamine (TEA, 0.20 mL) was added to the solution. The white precipitate (TEA·HCl) was removed by filtration. The filtrate was mixed with $Cu(OAc)_2 \cdot H_2O$ (144 mg) in DMF (6 mL), and the solution color turned blue-violet within 10 min (solution A). $H_2$5-Br-*m*BDC (36 mg) dissolved in DMF (2.4 mL) was mixed with solution A (2.2 mL) in a capped vial (20 mL) and heated at 85 °C for 14 h. Green cubic crystals were formed. These crystals were washed with 3 ×

(13) (a) Hanson, M. P.; Marvel, C. S. *J. Polym. Sci., Polym. Lett. Ed.* **1978**, *16*, 653–656. (b) Lin, S.-C.; Marvel, C. S. *J. Polym. Sci., Polym. Chem. Ed.* **1979**, *17*, 2337–2350. (c) Kwong, C.-Y.; Chan, T.-L.; Chow H.-F.; Lin, S.-C.; Leung, M.-K. *J. Chin. Chem. Soc.* **1997**, *44*, 211–224.
(14) Yoshino, T.; Nagata, Y.; Itoh, E.; Hashimoto, M.; Katoh, T.; Terashima, S. *Tetrahedron Lett.* **1996**, *37*, 3475–3478.
(15) Francisca Mary, L. J.; Kannan, P. *Eur. Polym. J.* **1999**, *35*, 17–26.
(16) Percec, V.; Lee, M.; Jonsson, H. *J. Polym. Sci., Part A: Polym. Chem.* **1991**, *29*, 327–337.
(17) Percec, V.; Zhao, M.; Bae, J.-Y.; Hill, D. H. *Macromolecules* **1996**, *29*, 3727–3735.
(18) (a) Musa, A.; Sridharan, B.; Lee, H.; Mattern, D. L. *J. Org. Chem.* **1996**, *61*, 5481–5484. (b) Connor, D. M.; Allen, S. D.; Collard, D. M.; Liotta, C. L.; Schiraldi, D. A. *J. Org. Chem.* **1999**, *64*, 6888–6890.
(19) Kraus, W.; Nolze, G. *J. Appl. Crystallogr.* **1996**, *29*, 301–303.
(20) Furukawa, H.; Miller, M. A.; Yaghi, O. M. *J. Mater. Chem.* **2007**, *17*, 3197–3204.

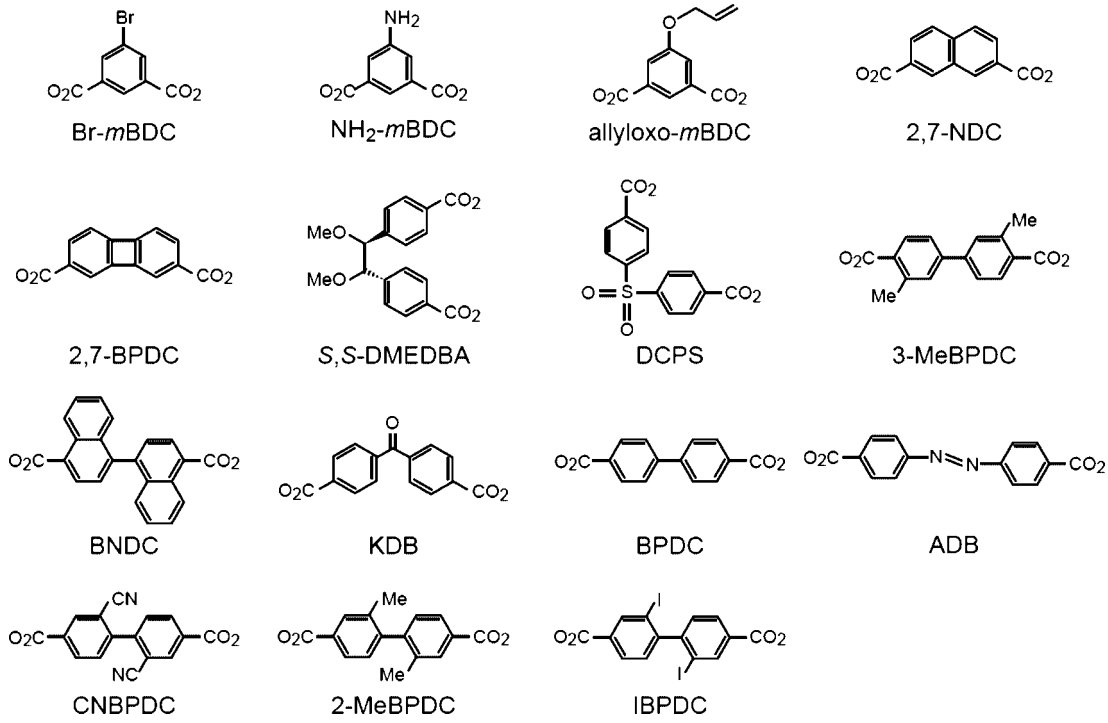

Figure 3. Structures of ditopic organic links and their abbreviations.

Table 1. Single Crystal X-ray Data for MOPs

MOP-*n*	organic link	chemical formula[a] space group; *a*, *b*, *c*, (Å); α, β, γ (deg); *V* (Å^3); *Z*
MOP-14	Br-*m*BDC	Cu_{24}(Br-*m*BDC)$_{24}$·(DMF)$_8$(Gly-*t*Bu)$_8$(H_2O)$_8$ *Im*$\bar{3}$*m*; 29.663, 29.663, 29.663; 90, 90, 90; 26 099; 2
MOP-15	NH_2-*m*BDC	Cu_{24}(NH_2-*m*BDC)$_{24}$·(DMF)$_{12}$(H_2O)$_{12}$ *I*4/*m*; 31.2356, 31.2356, 30.617; 90, 90, 90; 29 872; 2
MOP-17	Allyloxo-*m*BDC	Cu_{24}(allyloxo-*m*BDC)$_{24}$·(EtOH)$_{12}$(DEF)$_6$(H_2O)$_6$ *Cmca*; 40.654, 39.940, 28.935; 90, 90, 90; 46 982; 4
MOP-23	2,7-NDC	Cu_{24}(2,7-NDC)$_{24}$·(DEF)$_8$(H_2O)$_{16}$ *Cmca*; 44.289, 39.490, 37.176; 90, 90, 90; 65 021; 4
MOP-24	2,7-BPDC	Cu_{24}(2,7-BPDC)$_{24}$·(NMP)$_{12}$(H_2O)$_{12}$ *R*$\bar{3}$*c*; 38.3867, 38.3867, 141.831; 90, 90, 120; 180 993; 6

[a] DMF = dimethylformamide; DEF = diethylformamide; EtOH = ethanol; NMP = 1-methyl-2-pyrrolidinone; Gly-*t*Bu = glycine *tert*-butyl ester.

2 mL of DMF, and 2 × 1 mL of cyclohexane (yield: 18 mg, 24% based on $H_2$5-Br-*m*BDC). Anal. Calcd for $C_{360}H_{512}O_{180}N_{48}Cu_{24}Br_{24}$ = Cu_{24}(5-Br-*m*BDC)$_{24}$(DMF)$_{40}$(Gly-*t*Bu)$_8$(H_2O)$_{28}$: C, 36.54; H, 4.36; N, 5.58%. Found: C, 36.52; H, 3.89; N, 5.85%. FT-IR: (KBr, 3500−400 cm^{-1}): 3443 (br), 3078 (w), 2934 (w), 2859 (w), 1708 (w), 1627 (s), 1561 (s), 1443 (s), 1378 (s), 1245 (w), 1108 (w), 904 (w), 776 (m), 731 (m), 664 (w).

Cu_{24}(5-NH_2-*m*BDC)$_{24}$(DMF)$_{12}$(H_2O)$_{12}$·(DMF)$_{32}$(EtOH)$_6$(H_2O)$_{12}$, MOP-15. Solution A was prepared by the same manner as that for MOP-14. $H_2$5-NH_2-*m*BDC (18 mg) dissolved in DMF/EtOH (2.6:0.4 mL) was mixed with solution A (3.0 mL) in a capped vial (20 mL) and maintained at room temperature for 5 days. Green truncated-octahedral crystals were formed. These crystals were washed with 3 × 10 mL of DMF and 2 × 5 mL of cyclohexane (yield: 13 mg, 31% based on $H_2$5-NH_2-*m*BDC). Anal. Calcd for $C_{358}H_{578}N_{74}O_{185}Cu_{24}$ = Cu_{24}(5-NH_2-*m*BDC)$_{24}$(DMF)$_{44}$(EtOH)$_6$(H_2O)$_{24}$: C, 41.40; H, 5.29; N, 9.77%. Found: C, 41.32; H, 5.22; N, 10.12%. FT-IR: (KBr, 3500−400 cm^{-1}): 3440 (br), 3355 (m), 3237 (w), 2932 (w), 2880 (w), 2819 (w), 1668 (s), 1630 (s), 1593 (s), 1435 (sh), 1387 (s), 1253 (w), 1099 (m), 1062 (w), 1003 (w), 960 (w), 898 (w), 776 (m), 735 (m), 663 (w), 555 (w), 493 (w).

Cu_{24}(5-allyloxo-*m*BDC)$_{24}$(EtOH)$_{12}$(DEF)$_6$(H_2O)$_6$·(DEF)$_{16}$, MOP-17. Equimolar amounts of $H_2$5-allyloxo-*m*BDC, (0.0187 g, 0.084 mmol) and $Cu(NO_3)_2$·2.5H_2O (0.019 g, 0.082 mmol) in a solvent mixture of DEF/ethanol (1.2:0.8 mL) were placed in a glass tube (10 mm diameter and 140 mm length). The tube was sealed under vacuum and heated at a constant rate of 1 °C min^{-1} to 100 °C for 20 h and then cooled at a constant rate of 0.1 °C min^{-1} to room temperature in a stepwise fashion (80 °C for 4 h and 60 °C for 4 h). The blue rhombic plate-shaped crystals were washed with 3 × 2 mL of DEF and 2 × 1 mL of cyclohexane (yield: 16 mg, 48% based on $H_2$5-allyloxo-*m*BDC). Anal. Calcd for $C_{398}H_{518}N_{22}O_{160}Cu_{24}$ = Cu_{24}(5-allyloxo-*m*BDC)$_{24}$(DEF)$_{22}$(EtOH)$_{12}$(H_2O)$_6$: C, 49.30; H, 5.39; N, 3.18%. Found: C, 49.55; H, 4.94; N, 3.38%. FT-IR: (KBr, 3500−400 cm^{-1}): 3440 (br), 3088 (w), 2982 (w), 2931 (w), 2380 (w), 2854 (w), 1632 (s), 1591 (s), 1459 (m), 1417 (m), 1388 (s), 1326 (w), 1276 (w), 1133 (w), 1047 (w), 934 (w), 777 (m), 735 (m).

Cu_{24}(2,7-NDC)$_{24}$(DEF)$_8$(H_2O)$_{16}$·(DEF)$_{20}$(EtOH)$_4$(H_2O)$_{14}$, MOP-23. Equimolar amounts of $H_2$2,7-NDC (0.0181 g, 0.084 mmol) and $Cu(NO_3)_2$·2.5H_2O (0.019 g, 0.082 mmol) in a solvent mixture of DEF/ethanol (1.5:0.5 mL) were placed in a glass tube (10 mm diameter and 140 mm length). The tube was sealed under vacuum and heated at a constant rate of 1 °C min^{-1} to 100 °C for 20 h and then cooled at a constant rate of 1 °C min^{-1} to room temperature. The blue prismatic crystals were washed with 3 × 2 mL of DEF and 2 × 1 mL of cyclohexane (yield: 27 mg, 74% based on $H_2$2,7-NDC). Anal. Calcd for $C_{436}H_{556}N_{28}O_{168}Cu_{24}$ = Cu_{24}(2,7-NDC)$_{24}$(DEF)$_{28}$(EtOH)$_4$(H_2O)$_{40}$: C, 50.34; H, 5.39; N, 3.77%. Found: C, 50.40; H, 4.99; N, 4.05%. FT-IR: (KBr, 3500−400 cm^{-1}): 3440 (br), 2982 (w), 2936 (w), 2875 (w), 1718 (w), 1637 (s), 1561 (w), 1510 (w), 1439 (s), 1398 (s), 1362 (s), 1270 (w), 1240 (w), 1215 (w), 1108 (w), 935 (w), 857 (w), 828 (w), 797 (m), 761 (w), 659 (w), 619 (w). For porosity measurements, as-synthesized MOP-23 was rinsed with DMF and immersed in tetrahydrofuran (THF) for 1 week, during which the activation solvent was decanted and freshly replenished three times. The solvent was removed under vacuum at room temperature, yielding porous material.

$Cu_{24}(2,7\text{-BPDC})_{24}(NMP)_{12}(H_2O)_{12}\cdot(NMP)_{52}(H_2O)_{16}$, MOP-24. Equimolar amounts of $H_2$2,7-BPDC (0.020 g, 0.084 mmol) and $Cu(NO_3)_2\cdot 2.5H_2O$ (0.019 g, 0.082 mmol) in a solvent mixture of NMP/H_2O (2.0:0.02 mL) were placed in a glass tube (10 mm diameter and 140 mm length). The tube was sealed under vacuum and heated at a constant rate of 1 °C min^{-1} to 80 °C for 20 h and then cooled at a constant rate of 0.1 °C min^{-1} to room temperature in a stepwise fashion (65 °C for 10 h and 50 °C for 10 h) and held at room temperature for 7 days. The green crystals were washed with 3 × 2 mL of NMP and 2 × 1 mL of cyclohexane (yield: 16 mg, 32% based on $H_2$2,7-BPDC). Anal. Calcd for $C_{656}H_{776}N_{64}O_{188}Cu_{24}$ = $Cu_{24}(2,7\text{-BPDC})_{24}(NMP)_{64}(H_2O)_{28}$: C, 55.92; H, 5.55; N, 6.36%. Found: C, 55.85; H, 5.65; N, 6.68%. FT-IR: (KBr, 3500−400 cm^{-1}): 3440 (br), 3068 (w), 2931 (w), 2880 (w), 1689 (s), 1614 (s), 1581 (w), 1504 (w), 1449 (w), 1399 (s), 1383 (s), 1298 (w), 1253 (w), 1114 (w), 980 (w), 840 (w), 775 (m), 685 (m), 563 (w), 472 (w).

$Cu_2(S,S\text{-DMEDBA})_2(H_2O)_2\cdot(DEF)_{0.5}(H_2O)_4$, MOF-222. Equimolar amounts of H_2S,S-DMEDBA (0.027 g, 0.082 mmol) and $Cu(NO_3)_2\cdot 2.5H_2O$ (0.020 g, 0.082 mmol) in a solvent mixture of DEF/EtOH/H_2O (2.5:3.0:3.0 mL) were placed in a capped vial (20 mL). The vial was heated at 85 °C for 3 days. Block-shaped blue crystals of MOF-222 were formed and isolated by washing with DMF/methanol (4 × 2 mL) and drying briefly in the air (yield: 15 mg, 35% based on H_2S,S-DMEDBA). Anal. Calcd for $C_{38.5}H_{49.5}O_{18.5}N_{0.5}Cu_2$ = $Cu_2(S,S\text{-DMEDBA})_2(H_2O)_6(DEF)_{0.5}$: C, 48.69; H, 5.53; N, 0.72%. Found: C, 48.32; H, 5.69; N, 1.09%. FT-IR: (KBr, 3500−400 cm^{-1}): 3436 (br), 2982 (w), 2936 (w), 1643 (m), 1617 (m), 1419 (vs), 1388 (s), 1358 (s), 1098 (w), 874 (w), 787 (w), 675 (s), 517 (w), 435 (w).

$Zn_2(DCPS)_2(DMF)_2\cdot(DMF)$, MOF-114. H_2DCPS (15 mg, 0.049 mmol) and $Zn(NO_3)_2\cdot 4H_2O$ (26 mg, 0.10 mmol) in 2 mL of DMF were placed in a capped vial (4 mL). The vial was heated at 100 °C for 20 h. The colorless prismatic crystals were washed with 3 × 2 mL of DMF and 2 × 1 mL of cyclohexane (yield: 16 mg, 66% based on H_2DCPS). Anal. Calcd for $C_{37}H_{37}N_3O_{15}S_2Zn_2$ = $Zn_2(DCPS)_2(DMF)_3$: C, 46.36; H, 3.89; N, 4.38; S, 6.69%. Found: C, 46.24; H, 3.92; N, 4.73; S, 6.46%. FT-IR: (KBr, 3500−400 cm^{-1}): 3440 (br), 3068 (w), 2936 (m), 2931 (w), 2773 (w), 2750 (w), 1673 (s), 1637 (s), 1571 (m), 1490 (w), 1413 (s), 1383 (sh), 1331 (m), 1306 (m), 1255 (w), 1166 (s), 1138 (m), 1107 (s), 1016 (w), 873 (w), 848 (w), 781 (m), 746 (s), 726 (m), 695 (m), 665 (w), 624 (m), 583 (w), 512 (m), 481 (w), 446 (w).

$Cu_2(3\text{-MeBPDC})_2(DMF)_2\cdot(DMF)$, MOF-115. $H_2$3-MeBPDC (20 mg, 0.074 mmol) and $Cu(NO_3)_2\cdot 2.5H_2O$ (20 mg, 0.086 mmol) in a solvent mixture of DMF/EtOH/H_2O (1.5:0.5:0.5 mL) were placed in a capped vial (4 mL). The vial was heated at 65 °C for 20 h. The blue block-shaped crystals were washed with 3 × 2 mL of DMF and 2 × 1 mL of cyclohexane (yield: 23 mg, 71% based on $H_2$3-MeBPDC). Anal. Calcd for $C_{41}H_{45}N_3O_{11}Cu_2$ = $Cu_2(3\text{-MeBPDC})_2(DMF)_3$: C, 55.66; H, 5.50; N, 4.33%. Found: C, 55.78; H, 5.14; N, 4.76%. FT-IR: (KBr, 3500−400 cm^{-1}): 3434 (br), 2956 (w), 2931 (m), 2890 (w), 2803 (w), 1667 (s), 1612 (s), 1500 (w), 1403 (s), 1255 (w), 1166 (w), 1103 (m), 1062 (w), 858 (m), 791 (m), 715 (w), 675 (m), 563 (w), 486 (m).

$Cu_2(BNDC)_2(Py)_2\cdot(DMF)_2(H_2O)$, MOF-116. Equimolar amounts of H_2BNDC (0.030 g, 0.088 mmol) and $Cu(NO_3)_2\cdot 2.5H_2O$ (0.020 g, 0.086 mmol) in a solvent mixture of DMF/MeOH/pyridine (6.0:2.0:0.35 mL) were placed in a capped vial (20 mL). The vial was heated at a constant rate of 1 °C min^{-1} to 80 °C for 20 h and then cooled at a constant rate of 1.0 °C min^{-1} to room temperature. The green block-shaped crystals were washed with 3 × 2 mL of DMF and 2 × 1 mL of cyclohexane (yield: 31 mg, 63% based on H_2BNDC). Anal. Calcd for $C_{60}H_{50}N_4O_{11}Cu_2$ = $Cu_2(BNDC)_2(DMF)_2(Py)_2(H_2O)$: C, 63.77; H, 4.46; N, 4.96%. Found: C, 64.01; H, 4.25; N, 4.93%. FT-IR: (KBr, 3500−400 cm^{-1}): 3434 (br), 3058 (w), 2925 (w), 2849 (w), 1673 (s), 1617 (s), 1576 (s), 1515 (m), 1413 (s), 1367 (s), 1260 (w), 1220 (w), 1153 (w), 1092 (w), 1042 (w), 1011 (w), 889 (w), 863 (w), 782 (m), 762 (m), 705 (m), 660 (m), 629 (w), 542 (w), 466 (w).

$Cu_2(KDB)_2(DEF)_2\cdot(DEF)_2$, MOF-117. Equimolar amounts of H_2KDB (0.0227 g, 0.084 mmol) and $Cu(NO_3)_2\cdot 2.5H_2O$ (0.019 g, 0.082 mmol) in 2 mL of DEF were placed in a glass tube (10 mm diameter and 140 mm length). The tube was sealed under vacuum and heated at 85 °C for 20 h. The green block-shaped crystals were washed with 3 × 2 mL of DEF and 2 × 1 mL of cyclohexane (yield: 18 mg, 40% based on H_2KDB). Anal. Calcd for $C_{50}H_{60}N_4O_{14}Cu_2$ = $Cu_2(KDB)_2(DEF)_4$: C, 56.22; H, 5.66; N, 5.25%. Found: C, 56.18; H, 5.52; N, 5.75%. FT-IR: (KBr, 3500−400 cm^{-1}): 3440 (br), 3073 (w), 2981 (w), 2941 (w), 2885 (w), 1678 (s), 1658 (s), 1622 (s), 1566 (w), 1505 (m), 1413 (s), 1306 (m), 1275 (m), 1214 (w), 1142 (w), 1113 (w), 1016 (w), 939 (m), 883 (w), 843 (m), 787 (w), 736 (m), 649 (w), 537 (w), 461 (w).

$Cu_2(BPDC)_2(Py)(MeOH)\cdot(DMA)_4(Py)(H_2O)_4$, MOF-118. Equimolar amounts of H_2BPDC (0.027 g, 0.11 mmol) and $Cu(NO_3)_2\cdot 2.5H_2O$ (0.026 g, 0.11 mmol) in a solvent mixture of DMA/MeOH/pyridine (1.5:0.5:0.05 mL) were placed in a glass tube (10 mm diameter and 140 mm length). The tube was sealed under vacuum and heated at a constant rate of 1 °C min^{-1} to 85 °C for 48 h and then cooled at a constant rate of 1.0 °C min^{-1} to room temperature. The blue block-shaped crystals were washed with 3 × 2 mL of DMF and 2 × 1 mL of cyclohexane (yield: 38 mg, 55% based on H_2BPDC). Anal. Calcd for $C_{55}H_{74}N_6O_{17}Cu_2$ = $Cu_2(BPDC)_2(DMA)_4(MeOH)(H_2O)_4(Py)_2$: C, 54.22; H, 6.12; N, 6.90%. Found: C, 53.60; H, 6.01; N, 7.16%. FT-IR: (KBr, 3500−400 cm^{-1}): 3436 (br), 3017 (w), 2931 (m), 1647 (s), 1607 (s), 1551 (w), 1500 (w), 1403 (s), 1264 (w), 1179 (m), 1106 (w), 1006 (m), 856 (w), 842 (w), 770 (s), 705 (w), 686 (m), 590 (w), 482 (m).

$Cu_2(ADB)_2(DMA)_2\cdot(DMA)(Py)(H_2O)_2$, MOF-119. Equimolar amounts of H_2ADB (0.006 g, 0.022 mmol) and $Cu(NO_3)_2\cdot 2.5H_2O$ (0.005 g, 0.021 mmol) in a solvent mixture of DMA/EtOH/pyridine (1.5:0.5:0.05 mL) were placed in a glass tube (10 mm diameter and 140 mm length). The tube was sealed under vacuum and heated at a constant rate of 1 °C min^{-1} to 85 °C for 40 h and then cooled at a constant rate of 1.0 °C min^{-1} to room temperature. The dark green rodlike crystals were washed with 3 × 2 mL of DMF and 2 × 1 mL of cyclohexane (yield: 5 mg, 42% based on H_2ADB). Anal. Calcd for $C_{45}H_{52}N_8O_{13}Cu_2$ = $Cu_2(ADB)_2(DMA)_3(Py)(H_2O)_2$: C, 51.97; H, 5.04; N, 10.77%. Found: C, 51.64; H, 4.33; N, 10.39%. FT-IR: (KBr, 3500−400 cm^{-1}): 3440 (br), 3063 (w), 2931 (w), 2854 (w), 1607 (s), 1571 (m), 1500 (w), 1403 (s), 1306 (w), 1266 (w), 1220 (w), 1103 (w), 1011 (m), 883 (m), 792 (s), 711 (m), 644 (w), 461 (m).

$Cu_2(CNBPDC)_2(DMF)_2\cdot(DMF)_2(NMP)(H_2O)_2$, MOF-601. Equimolar amounts of H_2CNBPDC (0.017 g, 0.058 mmol) and $Cu(NO_3)_2\cdot 2.5H_2O$ (0.013 g, 0.056 mmol) in a solvent mixture of DMF/NMP (1.5:0.5 mL) were placed in a glass tube (10 mm diameter and 140 mm length). The tube was sealed under vacuum and heated at 85 °C for 20 h. The blue block-shaped crystals were washed with 3 × 2 mL of DMF and 2 × 1 mL of cyclohexane (yield: 16 mg, 63% based on H_2CNBPDC). Anal. Calcd for $C_{49}H_{53}N_9O_{15}Cu_2$ = $Cu_2(CNBPDC)_2(DMF)_4(NMP)(H_2O)_2$: C, 51.85; H, 4.71; N, 11.11%. Found: C, 51.75; H, 4.56; N, 11.37%. FT-IR: (KBr, 3500 − 400 cm^{-1}): 3435 (br), 3068 (w), 2936 (w), 2875 (sh), 2814 (w), 2233 (m), 1663 (s), 1551 (w), 1500 (w), 1418 (s), 1388 (s), 1255 (w), 1199 (w), 1103 (w), 1014 (w), 930 (w), 863 (w), 777 (m), 675 (w), 599 (w), 558 (w), 476 (w). For porosity measurements, as-synthesized MOF-601 was rinsed with DMF and immersed in THF for a week, during which the activation solvent was decanted and freshly replenished three times. The solvent was removed under vacuum at room temperature, yielding porous material.

$Cu_2(2\text{-MeBPDC})_2(DMA)_2\cdot(DMA)_2(DMF)(Py)(H_2O)_3$, MOF-602. Equimolar amounts of $H_2$2-MeBPDC (0.010 g, 0.037 mmol) and $Cu(NO_3)_2\cdot 2.5H_2O$ (0.0084 g, 0.036 mmol) in a solvent mixture of DMA/DMF/pyridine (1.3:0.7:0.01 mL) were placed in a glass tube (10 mm diameter and 140 mm length). The tube was sealed

under vacuum and heated at 85 °C for 30 h. The blue block-shaped crystals were washed with 3 × 2 mL of DMF and 2 × 1 mL of cyclohexane (yield: 13 mg, 57% based on $H_2$2-MeBPDC). Anal. Calcd for $C_{55}H_{78}N_6O_{16}Cu_2$ = Cu_2(2-MeBPDC)$_2$(DMA)$_4$(DMF)(Py)-(H_2O)$_3$: C, 54.21; H, 6.45; N, 6.90%. Found: C, 55.03; H, 6.37; N, 6.88%. FT-IR: (KBr, 3500 − 400 cm^{-1}): 3440 (br), 3022 (w), 2931 (w), 2809 (sh), 1714 (w), 1653 (s), 1607 (s), 1556 (w), 1510 (w), 1413 (s), 1266 (w), 1189 (w), 1011 (m), 909 (w), 853 (w), 787 (m), 736 (w), 685 (w), 594 (w), 482 (w). For porosity measurements, as-synthesized MOF-602 was rinsed with DMA and immersed in THF for a week, during which the activation solvent was decanted and replenished with fresh solvent three times. The solvent was removed under vacuum at room temperature, yielding porous material.

Cu_2(IBPDC)$_2$(Py)$_{1.67}$(H_2O)$_{0.33}$·(DMF)$_2$(H_2O)$_{2.33}$, MOF-603. Equimolar amounts of H_2IBPDC (0.022 g, 0.042 mmol) and Cu(NO_3)$_2$·2.5H_2O (0.010 g, 0.043 mmol) in a solvent mixture of DMF/EtOH/pyridine (1.5:0.5:0.07 mL) were placed in a glass tube (10 mm diameter and 140 mm length). The tube was sealed under vacuum and heated at 85 °C for 20 h. The blue block-shaped crystals were washed with 3 × 2 mL of DMF and 2 × 1 mL of cyclohexane (yield: 24 mg, 76% based on H_2IBPDC). Anal. Calcd for $C_{42.33}H_{39.67}N_{3.67}O_{12.67}Cu_2I_4$ = Cu_2(IBPDC)$_2$(DMF)$_2$(H_2O)$_{2.67}$-(Py)$_{1.67}$: C, 35.38; H, 2.78; N, 3.57%. Found: C, 35.16; H, 2.70; N, 3.38%. FT-IR: (KBr, 3500 − 400 cm^{-1}): 3440 (br), 3063 (w), 2926 (w), 2861 (sh), 1662 (s), 1622 (s), 1541 (m), 1396 (s), 1250 (w), 1103 (w), 1037 (w), 1001 (w), 853 (w), 782 (s), 708 (m), 660 (w), 475 (w). For porosity measurements, as-synthesized MOF-603 was rinsed with DMF and immersed in THF for a week, during which the activation solvent was decanted and freshly replenished three times. The solvent was removed under vacuum at room temperature, yielding porous material.

Cu_2(3-MeBPDC)$_2$(DMF)$_2$, MOF-604. $H_2$3-MeBPDC (20 mg, 0.074 mmol) and Cu(NO_3)$_2$·2.5H_2O (20 mg, 0.086 mmol) in a solvent mixture of DMF/EtOH/H_2O (1.5:0.5:0.5 mL) were placed in a capped vial (4 mL). The vial was heated at 65 °C for 20 h.

Table 2. Single Crystal X-ray Data for MOFs

MOF-*n*	organic link	chemical formula[a] space group; *a*, *b*, *c*, (Å); α, β, γ (deg); *V* (Å^3); *Z*
MOF-222	*S*,*S*-DMEDBA	Cu_2(*S*,*S*-DMEDBA)$_2$·(H_2O)$_2$ $P4_22_12$; 15.3277, 15.3277, 24.3220; 90, 90, 90; 5714.2; 4
MOF-114	DCPS	Zn_2(DCPS)$_2$·(DMF)$_2$ *C*2/*c*; 22.241, 12.7034, 17.6543; 90, 126.361, 90; 4016.8; 4
MOF-115	3-MeBPDC	Cu_2(3-MeBPDC)$_2$·(DMF)$_2$ *C*2/*m*; 13.220, 15.123, 11.734; 90, 105.673, 90; 2258.7; 2
MOF-116	BNDC	Cu_2(BNDC)$_2$·(Py)$_2$ *C*2/*m*; 13.7184, 20.3881, 9.3906; 90, 93.442, 90; 2621.7; 2
MOF-117	KDB	Cu_2(KDB)$_2$·(DEF)$_2$ $P2_1/c$; 10.0679, 18.449, 14.567; 90, 104.786, 90; 2616.1; 2
MOF-118	BPDC	Cu_2(BPDC)$_2$·(Py)(MeOH) *C*2; 24.4260, 17.8487, 15.1401; 90, 90.0360, 90; 6600.7; 4
MOF-119	ADB	Cu_2(ADB)$_2$·(DMA)$_2$ *Ibam*; 10.0482, 18.2409, 26.895; 90, 90, 90; 4929.6; 4
MOF-601	CNBPDC	Cu_2(CNBPDC)$_2$·(DMF)$_2$ $R\bar{3}m$; 44.0047, 44.0047, 12.2617; 90, 90, 120; 20562.7; 9
MOF-602	2-MeBPDC	Cu_2(2-MeBPDC)$_2$·(DMA)$_2$ $R\bar{3}m$; 46.3352, 46.3352, 10.4693; 90, 90, 120; 19465.7; 9
MOF-603	IBPDC	Cu_2(IBPDC)$_2$·(Py)$_{1.67}$(H_2O)$_{0.33}$ *C*2/*m*; 30.1786, 39.4019, 26.5077; 90, 120.9310, 90; 27037.6; 12
MOF-604	3-MeBPDC	Cu_2(3-MeBPDC)$_2$·(DMF)$_2$ *C*2/*c*; 24.1636, 17.6710, 10.1065; 90, 113.969, 90; 3943.3; 4

[a] DMA = dimethylacetamide; MeOH = methanol; Py = pyridine.

Results and Discussion

In this section, we describe the structures of MOPs and MOFs (Tables 1 and 2) in terms of the angles between the carboxylates as shown in Figure 1 which illustrates the four principal modes of distortion from the reference geometry (Figure 1A).

MOP-14 and 15 (Linker R-*m*BDC, R = Br and NH_2). Crystals of MOP-14 are composed of large discrete molecules constructed from the square building blocks bridged by organic links (Figure 4A); 12 square (Cu_2(–CO_2)$_4$) units are joined by 24 bromo-functionalized links (Br-*m*BDC) bent at an angle of 120° (180° is straight). Ideally, the square units are expected to have a total of 24 terminal ligands (8 DMF, 8 Gly-*t*Bu, and 8 water); however these were not fully resolved in the electron density maps of the crystal structure. However, the identity of the terminal ligands was confirmed from elemental analysis and TGA data. The simplest way to view this structure is comparison against the great rhombicuboctahedron (**cuo-a**[21]), where each square and link have been replaced by the square building blocks and the Br-*m*BDC units, respectively, to give a 26-faceted Archimedean solid (4.6.8 Archimedean polyhedron). The polyhedral framework of MOP-14 is isoreticular (having the same topology) to that of MOP-1 and other functionalized MOPs.[8] The structural isomer of a great rhombicuboctahedron in which connectivity is slightly different[8c,f] was not observed. The average diameter of the open cavity within this great rhombicuboctahedral MOP is 13.8 Å with an associated volume of 1380 Å^3. Each MOP-14 cage has eight nearest neighbors (i.e., *bcc*).

MOP-15 is isoreticular to MOP-14, differing only in the amine functional group attached to the benzene ring (NH_2-*m*BDC). A total of 24 terminal ligands (12 DMF and 12 H_2O on the external and internal faces of the squares) for MOP-15 were identified by single crystal X-ray data. The unit cell parameters of MOP-15 are similar to that of MOP-14; however, the overall structure of MOP-15 has lower tetragonal symmetry ($I4/m$, *bcc* packing) than that of the cubic MOP-14 structure ($Im\bar{3}m$). Since the closest midpoint distance of N−H···N was ca. 2.4 Å, we know that there are significant H-bonding interactions between nearest polyhedral neighbors and they are slightly rotated when compared to the positions of the polyhedra in MOP-14.

MOP-17 (Linker allyloxo-*m*BDC). Crystals of MOP-17 have 24 allyloxo-*m*BDC links (Figure 3) and 12 square (Cu_2(–CO_2)$_4$) units, whose core is again identical to that of MOP-1. Ethanol ligands (12) point away from the surface of the polyhedron while six water and six DEF ligands point toward the center of the polyhedron. Since the allyloxo groups protrude from the MOP surface, their orientation can be optimized to minimize steric repulsions between the alkyl chains. The distance between nearest neighbor vinyl groups of the neighboring MOF is ∼4 Å, indicating that the orientation of terminal vinyl groups is not favorable for solid-state photopolymerization reactions. Despite this, the alkyl chains still have a fair degree of flexibility, and there are apparently no interactions between the oxygen atom in the 5-position and the square unit of the adjacent

(21) Delgado-Friedrichs, O.; O'Keeffe, M.; Yaghi, O. M. *Phys. Chem. Chem. Phys.* **2007**, *9*, 1035–1043.

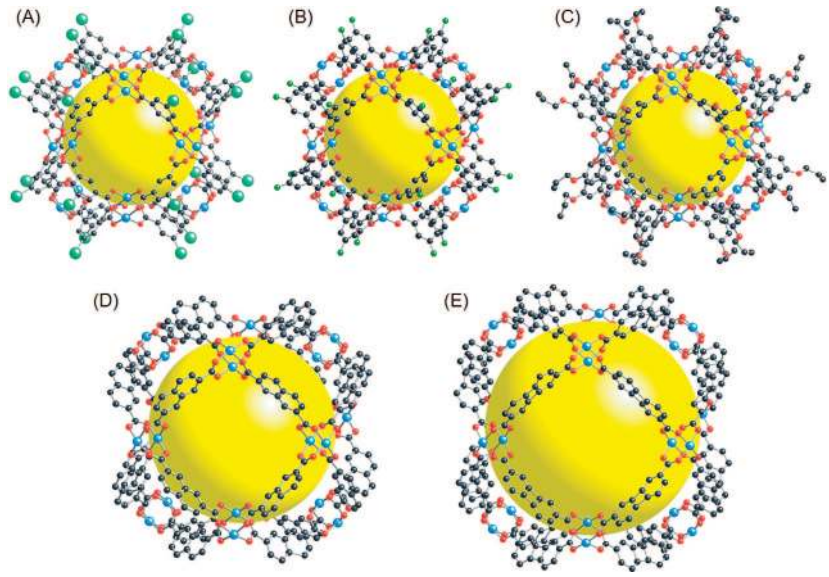

Figure 4. X-ray single crystal structures of a series of MOP compounds: (A) MOP-14, (B) MOP-15, (C) MOP-17, (D) MOP-23, and (E) MOP-24. The yellow sphere within each polyhedron represents the size of the largest sphere that would occupy the cavity without contacting the interior van der Waals surface. Cu, blue; O, red; C, black; Br, large green; N, green; all hydrogen atoms and terminal ligands on the square units are omitted for clarity.

polyhedron.[8e] MOP-17 is slightly soluble in DMA, although the solubility was much lower than that of MOP-18, whose surface is decorated by 24 dodecoxy chains.[8b] From this we hypothesize that longer aliphatic chains attached to an MOP surface could become a fruitful technique for the dissolution of these unique molecules.

MOP-23 and -24 (Linkers = 2,7-NDC and 2,7-BPDC). Crystals of MOP-23 (Figure 4D) are also composed of discrete molecular polyhedra constructed from square units and rigid organic links. As with the other MOPs discussed here, it is isoreticular with MOP-1 but now bridged by 2,7-NDC units (Figure 4). The square units are axially coordinated by a total of 24 species, 8 DEF, and 16 water molecules. The polyhedron has 8 triangular and 6 square apertures that are 6.0 and 9.2 Å across, respectively. The average diameter of the open cavity within this polyhedron is ca. 18.8 Å, and its void volume is more than twice that of the MOP-14 analogue. The distance between nearest naphthalene rings of neighboring polyhedron (midpoint distance between two carbons) is 3.2 Å, indicating that these polyhedra are quite close to each other. However, there were no identifiable hydrogen bonding interactions between these neighboring polyhedra. MOP-24 (R = 2,7-BPDC) is even larger than the MOP-23 (R = 2,7-NDC) polyhedra (Figure 4) while again maintaining the same topology. The average diameter of the open cavity within this polyhedron is ca. 21.6 Å. Here we note that the volume of MOP-24 (ca. 5270 $Å^3$) is nearly twice that of MOP-23 and four times as large as that of MOP-1.[8a] The paddlewheel units of these molecules have a total of 24 axial ligand: 12 coordinated NMP and 12 water molecules on the external and internal faces of the $Cu_2(-CO_2)_4$ paddlewheels. MOP-24 has a hexagonally packed structure in layers normal to the *c*-axis with the layers stacked along *c* in an ABC fashion so the packing is topologically cubic close packing, unlike other MOPs.

MOF-114 and 222 (Linkers = DCPS and *S,S*-DMEDBA). MOF-114 and -222 both have a 1-periodic structure (Figure 5). The synthesis of MOF-114 was accomplished by linking the Zn square unit (i.e., $Zn_2(-CO_2)_4$) with a link with an in-plane bend of 103.3°, fairly close to the ideal 90° for producing a 1-D chain (see Figure 1). Four carboxylate groups of four DCPS links bridge two zinc centers to form a structure with a Zn···Zn intrapaddlewheel distance of 2.95 Å. Each Zn is also coordinated by a terminal DMF molecule to result in a slightly distorted square pyramidal geometry. In MOF-222 Cu square units ($Cu_2(-CO_2)_4$) are bridged by a bent *S,S*-DMEDBA link, and two water molecules are coordinated at the axial positions of the square unit. The angle between two benzene rings is 47.1°, which is significantly smaller than the required angle 90° for the ideal geometry. To accommodate this, the plane formed by carboxylates (O−C−O) is tilted by 20.1° against two Cu atoms in the square unit. As a result, a dihedral angle between two triangles composed of two Cu atoms and a carboxylic carbon is 86.0°, close to the ideal angle. Indeed, in similar 1-D structures with a square unit linked by 1,4-cyclohexanedicarboxylate (M = Co, Ni, Zn), 2,2′-dithiodibenzenecarboxylate (M = Zn), (*S*)-2,2′-dihydroxy-1,1′-binaphthalene-6,6′-dicarboxylate (M = Zn), and 2,2′-biphenyldicarboxylate (M = Cu),[22] the values of the bend angle vary from 76.5° to 103.3°. It is apparent that a strict link geometry requirement is not necessary if the link has enough flexibility to form a 1-D structure.

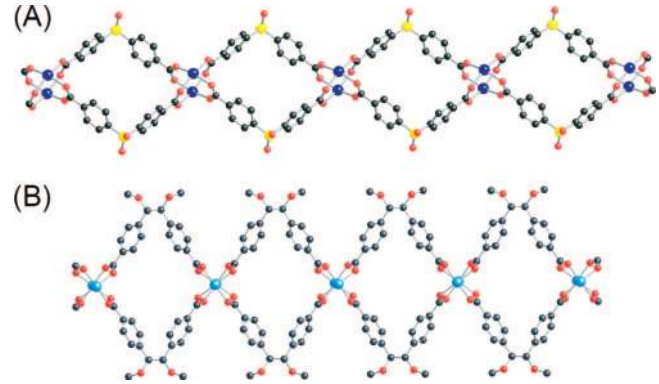

Figure 5. X-ray single crystal structures of MOF-114 (A) and MOF-222 (B). Zn, dark blue; Cu, blue; O, red; C, black; S, yellow; all hydrogen atoms and terminal ligands on the square units are omitted for clarity.

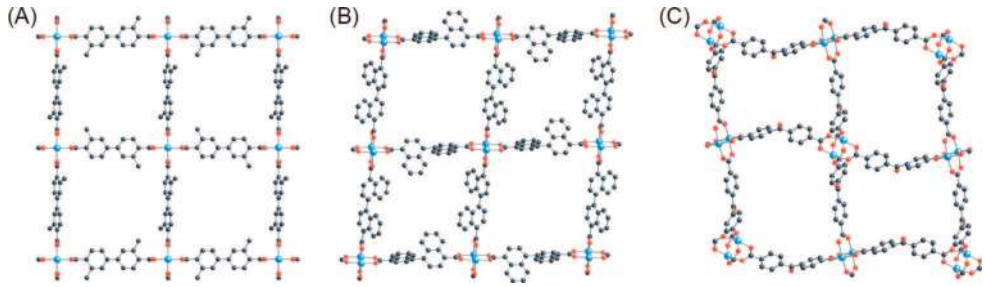

Figure 6. X-ray single crystal structures of MOF-115 (A), MOF-116 (B), and MOF-117 (C). Atom colors are the same as those in Figure 4.

MOF-115 - 117 (linkers = 3-MeBPDC, BNDC and KDB). MOF-115−117 have the 2-periodic 4^4 square lattice topology (**sql**-**a** = **fes**[21]), as in the MOF-2 structure (Figure 6).[6]

In MOF-115 square ($Cu_2(-CO_2)_4$) units are connected through a 3-MeBPDC link and two DMF molecules are coordinated at the axial positions of the square unit. For each 4^4-grid, two 3-MeBPDC links are located on opposing ends, lay parallel to the *b*-axis with a small dihedral angle between the carboxylate group and the biphenyl ring (21.8°), while the other two links are almost perpendicular to the vertical line of the square plane. The biphenyl rings are almost coplanar, and this unique conformation can be attributed to the steric hindrance between the two methyl groups in the same layer, which suggests that the angle between the carboxylate and benzene ring of the link can be controlled by the functionality of the ortho-position. These layers are stacked in a staggered manner to avoid unfavorable steric repulsions between the layers.

The structures of MOF-116 and MOF-117 (Figure 6) are also based on the 2-periodic **sql** net and illustrate the observation (see Figure 1E) that this net can be obtained for linkers of complex geometry. In MOF-117 the layers are very corrugated and can be seen from the figure.

Examination of the crystal structure of MOF-116 revealed the presence of 2 pyridine ligands per square ($Cu_2(-CO_2)_4$) unit. To minimize steric hindrance, two binaphthyl rings of BNDC are arranged in a near-orthogonal arrangement. The 2-D rhombohedral grids have dimensions of 15.2 × 15.2 Å^2 and again are stacked in a staggered manner with the closest C···C distance between neighboring layers of 3.6 Å. The trends are reminiscent of 2-D layers formed by binaphthylene dicarboxylic acid derivatives.[23]

The bent links in MOF-117 adopt the 4^4-grid topology by bending alternately above and below the plane of the grids[3,24] to produce corrugated sheets. Two included DEF molecules are identified by single X-ray diffraction data. The corrugated net obtained for MOF-117 is similar to that reported earlier for MOF-109 due to same organic link. However, in MOF-117, the corrugated sheets are stacked alternately; consequently, the distance between layers is shorter than that in MOF-109, in which the layers stack in an eclipsed fashion.[3]

MOF-118 and -119 (Linkers = ADB and BPDC). In contrast to MOF-115 to -117, the structures of MOF-118 and -119 contain interpenetrating square nets (Figure 7). Such interpenetrating 2-D nets with square building blocks are rare, because the dimensions of the square unit (including terminal ligands) are typically too large to allow interpenetration.

In MOF-118, the square unit is completed by four BPDC links to form a 4^4-grid with dimensions of 15.1 × 15.1 Å^2; the two benzene rings in the square are slightly tilted with respect to each other. Terminal methanol and pyridine ligands are also bound to the Cu atoms. This structure might be contrasted to that of MOF-106, which has distorted square grids composed of iron square units ($Fe_2(-CO_2)_4$) and somewhat bent BPDC links.[3] The 2-D sheets of MOF-118 interpenetrate one another in a parallel−parallel fashion,[25] whereas MOF-106 is not an interpenetrating structure. The angle between interpenetrating layers is 71.5°, and two benzene rings in neighboring 2-D sheets are close to each other (ca. 3.3 Å) and interlock the crystal structure through $\pi-\pi$ stacking. Given that the volume per square unit (i.e., unit cell volume/Z = 1649 Å^3) is larger than other 2-D compounds (1240 Å^3 for MOF-106; 1133 Å^3 for MOF-115), the reason why these square grids are packed loosely may be the $\pi-\pi$ interactions even though MOF-118 is an interpenetrating structure.

MOF-119, whose link contains an azo group between two benzene rings, assumes a diagonal−diagonal interpenetrating mode.[25] Square units are connected by four ADB links to form 2-D rhombohedral grids with terminal DMA ligands. The dimension of rhombohedral grids is 17.0 × 17.0 Å^2, and the angle between two ADB links is 75.5°. The rhombohedral nets form an oblique interpenetrating structure; the angle between the nets is 122.3°. Since the square unit of the second net is placed in the center of the rhombohedral grid, no specific interaction with neighboring 2-D sheets is observed.

MOF-601−603 (Linker = R-BPDC; R = CN, Me, and I). The crystals of MOF-601 to -603 were deliberately designed to have an NbO framework (**nbo**, Figure 2) by using 2,2′-R-BPDC (R = CN, Me, and I) whose angle between two carboxylates in BPDC derivatives is almost perpendicular due to bulky functional groups. In the MOF-601 structure each square unit is composed of four CNBPDC links and two axial DMF ligands. Because of the large twist (84.5°) in the CNBPDC link the neighboring Cu square units are almost perpendicular, which leads to an **nbo**-like extended network.[10] The second **nbo** framework is displaced by (1/4, 1/4, 1/4) relative to the first one so that the large hexagonal channels appear along the *c*-axis

(22) (a) Gong, Y.; Hua, C. W.; Lia, H.; Huang, K. L.; Tang, W. *J. Solid State Chem.* **2005**, *178*, 3152–3158. (b) Wang, S.; Mao-Lin, H.; Chen, F. *Acta Crystallogr.* **2004**, *E60*, m413–m415. (c) Cui, Y.; Ngo, H. L.; White, P. S.; Lin, W. *Chem. Commun.* **2003**, 994–995. (d) Kumagai, H.; Inoue, K.; Kurmoo, M. *Bull. Chem. Soc. Jpn.* **2002**, *75*, 1283–1289.

(23) Cui, Y.; Evans, O. R.; Ngo, H. L.; White, P. S.; Lin, W. *Angew. Chem., Int. Ed.* **2002**, *41*, 1159–1162.

(24) Kondo, M.; Irie, Y.; Shimizu, Y.; Miyazawa, M.; Kawaguchi, H.; Nakamura, A.; Naito, T.; Maeda, K.; Uchida, F. *Inorg. Chem.* **2004**, *43*, 6139–6141.

(25) Carlucci, L.; Ciani, G.; Proserpio, D. M. *Coord. Chem. Rev.* **2003**, *246*, 247–289.

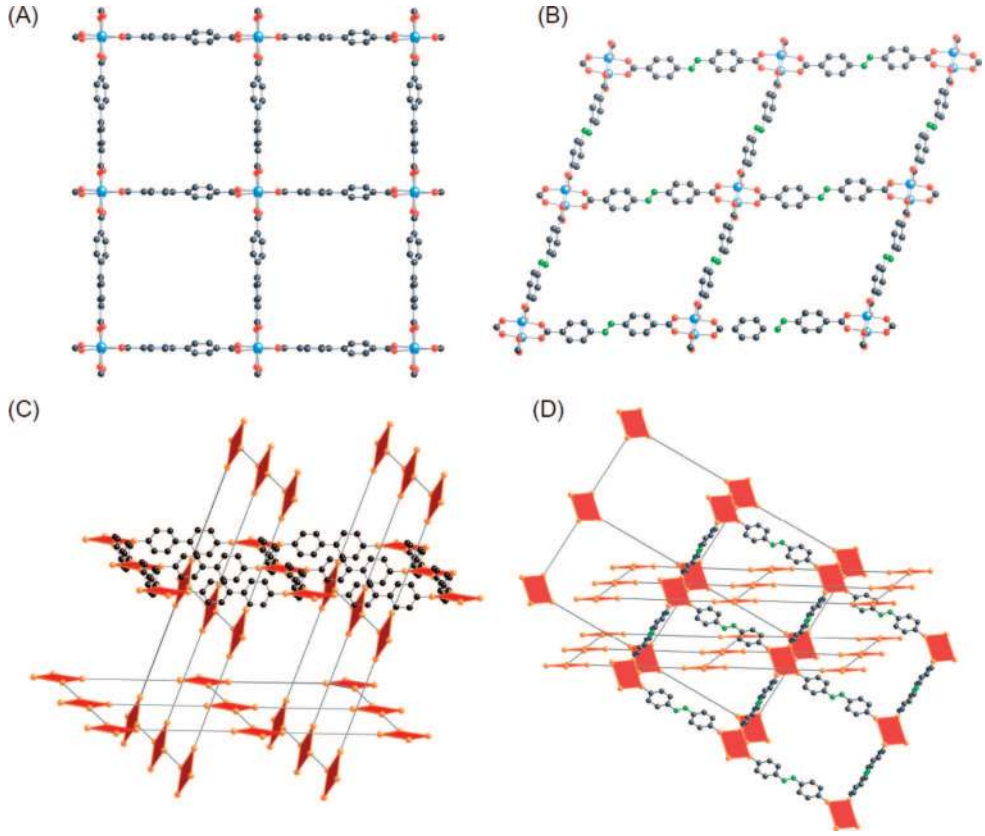

Figure 7. X-ray single crystal structures of MOF-118 (A) and MOF-119 (B) and the arrangement of interpenetrated layers in each (C, D). Atom colors are the same as in those Figure 4.

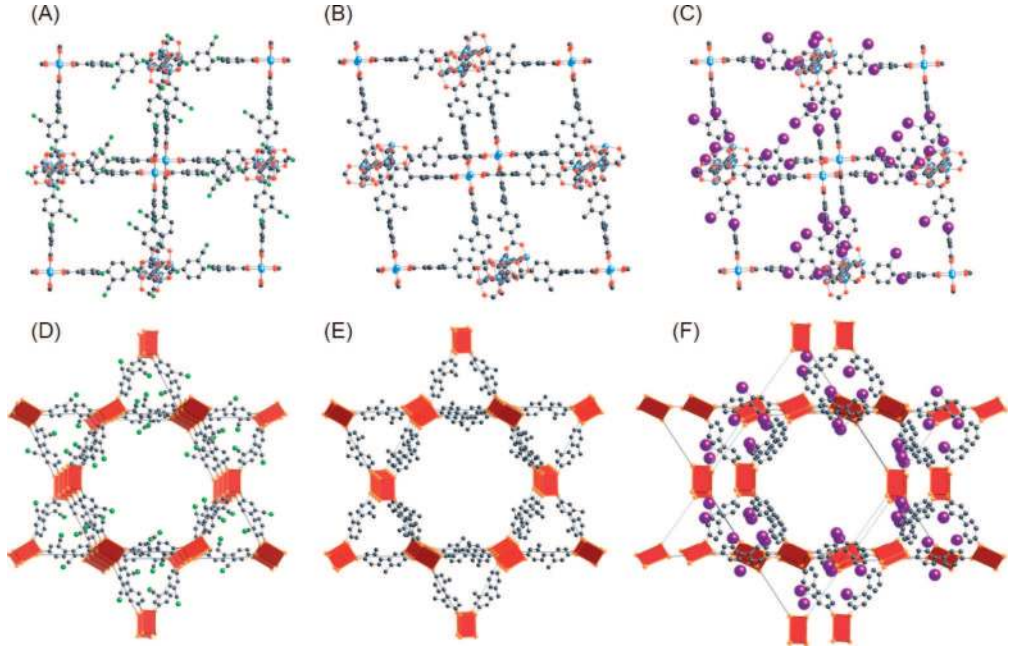

Figure 8. X-ray single crystal structures of **nbo** type frameworks for MOF-601 (A), MOF-602 (B), and MOF-603 (C) (only single framework is shown for clarity). Their doubly interpenetrating structures are shown in (D)−(F). Atom colors; Cu, blue; O, red; C, black; N, green; I, purple; all hydrogen atoms and terminal ligands on the paddlewheel units are omitted for clarity.

(Figure 8).[26] From the electron density map one-half of the CN groups (site occupancy factor (SOF) = 0.50) point toward the center of the 1-D channels while the remainder point toward the center of the triangular pores. The diameter of the channel of MOF-601 is estimated to be 15.2 Å.

The difference between the structures of MOF-601 and MOF-602 is only the functional groups on the biphenyl ring. The unit

(26) (a) Chen, B.; Fronczek, F. R.; Maverick, A. W. *Chem. Commun.* **2003**, 2166–1267. (b) Bu, X.-H.; Tong, M.-L.; Chang, H.-C.; Kitagawa, S.; Batten, S. R. *Angew. Chem., Int. Ed.* **2004**, *43*, 192–195.

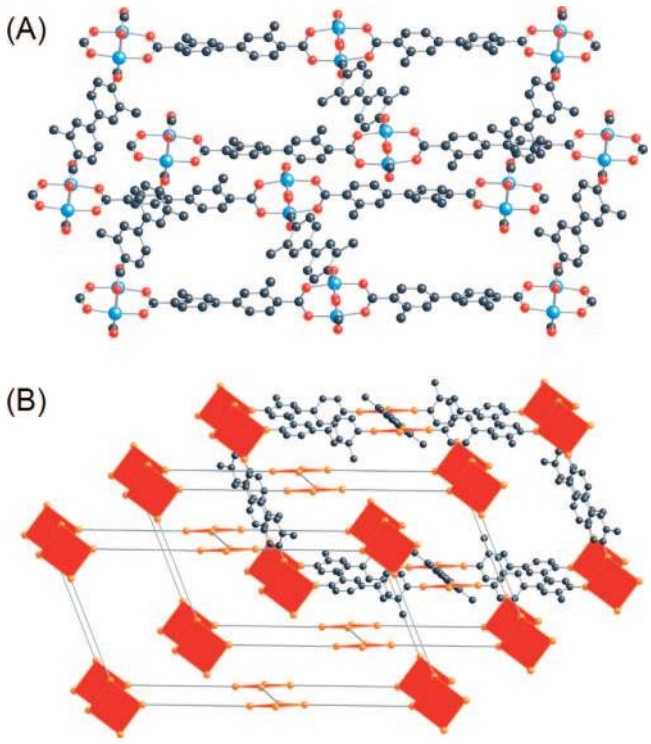

Figure 9. X-ray single crystal structures of **cds** type framework for MOF-604 (A) (only single framework is shown for clarity). Interpenetrating structure of MOF-604 is shown in (B). Atom colors are the same as those in Figure 4.

cell parameters of both are similar; however, the twist angle (75.3°) in MOF-602 is smaller than that in MOF-601, and therefore a unit cell length of the *c*-axis is slightly shorter than that for MOF-601. This is probably a result from steric hindrance of methyl groups in the triangular pores with the result that the occupancy of Me groups for hexagonal 1-D channels is 0.634, which is higher than that in MOF-601. One-dimensional channels of 15.2 × 15.2 Å^2 in which methyl groups and terminal DMA ligands protrude run along the *c* direction. It is worth noting that crystals of MOF-601 and -602 have a large internal void space in spite of their interpenetrated structures.

Replacement of the functional groups by heavy atoms (iodine) also yields an **nbo** net. In the case of MOF-603, two iodo groups give a twist angle of 86.3° which is still sufficient to form the **nbo** net comprising the Cu square units. In contrast to MOF-601 and -602, MOF-603 has an interwoven structure to mitigate steric repulsion between two pyridine molecules on the square unit. Consequently MOF-603 has only a single 1D pore with a diameter of 8.7 Å observed along the *c*-axis. This finding indicates that the difference in the catenation mode (i.e., interwoven structure) could reduce accessible volume for MOF-603, although the cell volume per square unit is larger than that of MOF-601 and -602.

MOF-604 (Linker = 3-MeBPDC). MOF-604 has the **cds** framework and was an unexpected contaminant in the product of the MOF-115 reaction. Since the **cds** net has two types of edges (S and T, Figure 2), two distinct sets of twist angles are required. The former S edge of the vertical line of the square unit is tilted against the carboxylate plane (46.6°) due to the methyl group on the BPDC. On the T edge, significant angles are observed between the two benzene rings (45.2°) as well as the carboxylate groups (27.8°) resulting in a total angle of 100.8°. The connectivity of MOF-604 is reminiscent of MOF-111.[3] This individual **cds** net has a large rectangular pore (ca. 15 × 30 Å^2), affording triple interpenetration of three discrete networks.[27,28]

Porosity and Architectural Stability. It is expected that MOFs based on the **nbo** topology will have enough space to take up large amounts of guest molecules. Therefore, we examined the gas sorption behavior of these samples, as well as MOP-23. These compounds were solvent-exchanged with THF and evacuated to remove free guest molecules; however, under these conditions the axial THF ligands on the square $(Cu_2(-CO_2)_4)$ units could not be removed without structural decomposition.[29] Upon desolvation of the exchanged material, decreased diffraction intensities and broadened reflections were observed in the PXRD pattern which indicates some loss of long-range order but not necessarily a loss of porosity. It should be noted that (110) diffraction lines for THF exchanged MOF-601 and -602 (2,2′-R-BPDC, R = CN and Me) were located at lower angles when compared with as-synthesized samples.[30] This may be because of framework expansion along the *c*-axis during solvent exchange.

N_2 sorption of MOP-23 (R = 2,7-NDC) followed a reversible type I isotherm at 77 K, which indicates that this compound possesses permanent porosity (Figure 10A). The apparent monolayer surface area and pore volume of MOP-23 were estimated from the N_2 adsorption data to be 860 m^2 g^{-1} (760 m^2 g^{-1} for BET model) and 0.34 cm^3 g^{-1}, respectively, and an uptake of 235 cm^3 g^{-1} can correspond to 70 N_2 molecules per truncated polyhedron (i.e., number of N_2 molecules/number of MOF cages).

The shape of the N_2 isotherm for MOF-601 (R = CNBPDC) is unique: it shows a very sharp uptake at a relative pressure, $P/P_0 < 0.01$, followed by a second step in the range from $P/P_0 = 0.03$ to 0.06. A similar step in the low pressure region was observed by Ar sorption at 77 and 87 K.[30] The P/P_0 values of the second step for Ar isotherms were higher than that of N_2. Since Ar has a smaller molecular volume, kinetic diameter, and polarity than N_2 it is reasonable to conclude that the second step is attributed to micropore filling and not a pore blocking mechanism. Similar steps are also observed by N_2 and Ar isotherms of MOF-602 (R = 2-MeBPDC). The relative pressure of N_2 and Ar filling in the micropore regions ($P/P_0 = 0.05-0.06$ and 0.07−0.09, respectively) are slightly larger than that in MOF-601 because of the somewhat larger pore diameter in MOF-602, which is decorated with methyl groups rather than cyano groups. The apparent surface area (S_{Lang}) of MOF-601 and -602 calculated from N_2 uptake of the first steps are 980 and 910 cm^2 g^{-1}, respectively. Estimated pore volumes based on a DR-plot method for MOF-601 and -602 are 0.47 and 0.53 cm^3 g^{-1}, respectively.

To estimate pore size distributions for MOF-601 and -602, Ar isotherms were analyzed using nonlocal density functional theory (NLDFT) implementing a hybrid kernel for Ar adsorption at 87 K based on a zeolite/silica model containing cylindrical pores.[31] The distribution calculated by fitting the MOF-601 and

(27) Delgado-Friedrichs, O.; O'Keeffe, M.; Yaghi, O. M. *Solid State Sci.* **2003**, *5*, 73–78.
(28) Batten, S. R.; Robson, R. *Angew. Chem., Int. Ed.* **1998**, *37*, 1460–1494.
(29) Typical activating solvents (e.g. chloroform, dichloromethane, acetone, acetonitrile) were also applied; however THF-activated materials had the most optimal performance.
(30) See Supporting Information for details.
(31) Ravikovitch, P. I.; Wei, D.; Chueh, W. T.; Haller, G. L.; Neimark, A. V. *J. Phys. Chem. B* **1997**, *101*, 3671–3679.

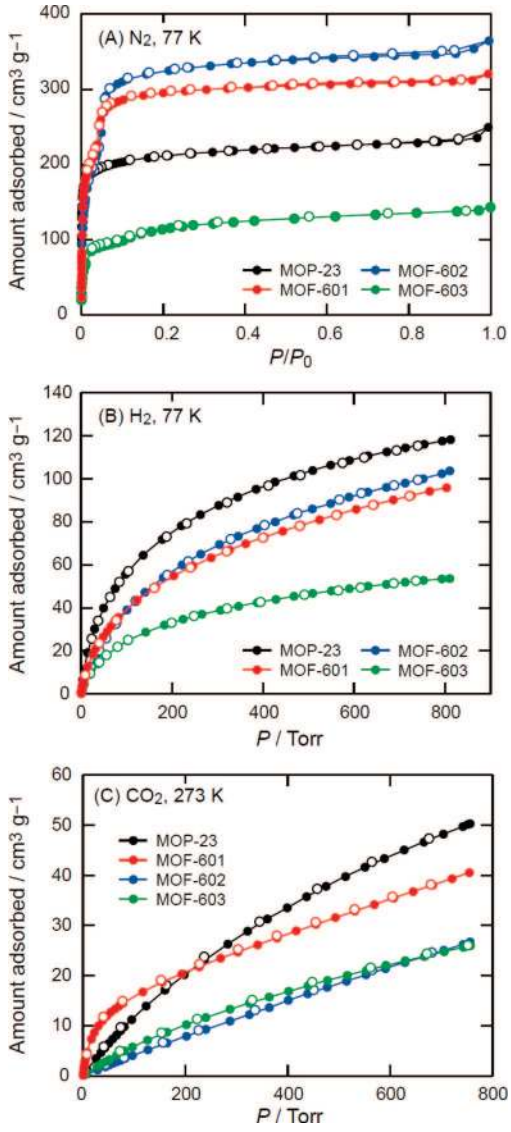

Figure 10. N_2 (A), H_2 (B), and CO_2 (C) adsorption isotherms for MOF-601 (red), MOF-602 (blue), MOF-603 (green), and MOP-23 (black). Filled and open circles represent adsorption and desorption branch, respectively. Connecting traces are guides for eyes.

-602 adsorption data revealed a narrow distribution of large pores with estimated diameters of 21.0 and 21.0 Å for MOF-601 and -602, respectively. These pore diameters are consistent with the *d*-spacing of powder XRD patterns for each of the respective activated materials[30] which are likely to possess 1-D open channels along the crystallographic *c* axes. This observation supports the notion that the pore diameters are large enough to exhibit micropore filling of N_2 and Ar in the low-pressure region of the isotherm.

The amount of N_2 uptake in MOF-603 (R = IBPDC) was less than one-half that of MOF-601 ($S_{Lang} = 430\ m^2\ g^{-1}$, $V_p = 0.20\ cm^3\ g^{-1}$), which may be attributed to the contribution of heavy iodo groups. This should not, however, be the reason for a faint step in the N_2 uptake between $P/P_0 = 0.1$ and 0.2 because usually such a step without hysteresis implies the existence of micropores and thus micropore filling. Although MOF-603 has a large cavity along the *c*-axis, the walls also contain small pores which allow small guest molecules to enter.

Interpenetration does not always have a negative impact on sorption properties, although there is the common idea that it would drastically reduce pore sizes and hence lead to a low capacity for gas storage. For instance, MOF-101 comprised of a noninterpenetrated **nbo** net did not show the permanent porosity as expected by the crystal structure due to a difficulty in sample activation.[10] This is in sharp contrast to interpenetrating **nbo** structures of MOF-601, -602, and -603. The findings suggest interpenetration should help reinforce the framework stability, even when employing long links.[32]

H_2 isotherms of MOP and MOFs measured at 77 K are shown in Figure 10B. The rapid pressure equilibration and absence of hysteresis confirm that H_2 is reversibly physisorbed in the MOP and MOF samples. However, under these conditions, H_2 isotherms are not fully saturated because of the low critical temperature of H_2 (33 K).[33] Consequently, the uptake of H_2 in the low pressure region does not depend on either the surface area or pore volume of the compounds.[34] In general, the chemical functionalities of the organic links are less effective for strong interaction with H_2, and therefore the H_2 uptake capacity should reflect the geometry of pore systems. In other words, the large internal void space for an **nbo**-type material is not effective for H_2 storage under low pressure.

Similarly, there is no specific relationship between CO_2 uptake and the surface area of the materials because of the large saturation pressure of CO_2 ($P_0 = 26\ 140$ Torr at 273 K).[33] MOF-601 (R = CNBPDC) exhibits a steep uptake in the low-pressure region, while MOF-602 (R = 2-MeBPDC) adsorbs only one-third of the amount of CO_2 at 200 Torr compared with MOF-601, despite the fact that MOF-602 has almost the same pore metrics and topology as MOF-601. The interaction of CO_2 with MOF-601 must therefore be stronger, and this effect is more important than the geometry of the pores in the low-pressure region. The reason for this may be seen by comparing the quadrupole moments of cyanobenzene and toluene, 16 and −8 B, respectively (1 B = 1 D·Å);[35] for example, the cyano groups in MOF-601 are more attractive to CO_2 (−4.3 B)[36] because of the quadrupole−quadrupole interaction. We would like to note that the inner surface of the 1-D channel is decorated with various chemical functional groups at the 2 and 2′ positions of the BPDC links. We believe this method for preparation of functionalized MOFs without changing the underlying framework (i.e., *isoreticular*) is a widely applicable technique which produces net based materials that can be utilized for the separation of relatively large molecules.

Concluding Remarks

We outlined the principles for construction of 0-D to 3-D architectures from various ditopic carboxylates and divalent metal ions. We have synthesized and characterized illustrative examples in which the topology between square ($Cu_2(-CO_2)_4$) paddlewheel units is dependent on specific linker angles. Rigid organic links of an appropriate bend angle (120°) preferentially yield polyhedral structures (MOPs). We have shown that the surfaces of MOPs can be easily functionalized without changing their underlying topology or the link geometry. When a linear

(32) Rowsell, J. L. C.; Yaghi, O. M. *Angew. Chem., Int. Ed.* **2005**, *44*, 4670–4679.
(33) NIST chemistry webbook (thermophysical properties of fluid systems); http://webbook.nist.gov/chemistry/fluid/.
(34) Frost, H.; Du1ren, T.; Snurr, R. Q. *J. Phys. Chem. B* **2006**, *110*, 9565–9570.
(35) (a) Kryachko, E. S.; Nguyen, M. T. *J. Chem. Phys.* **2001**, *115*, 833–841. (b) Pérez-Casas, S.; Hernández-Trujillo, J.; Costas, M. *J. Phys. Chem. B* **2003**, *107*, 4167–4174.
(36) Jiang, J.; Sandler, S. I. *J. Am. Chem. Soc.* **2005**, *127*, 11989–11997.

link is employed to join the square units, the twist angle plays a crucial role in determining both the dimensionality and topology of the final structure. Thus, in principle, the bulkiness of the chemical functional groups is only needed to adjust the twist angle and that linker length is not necessarily a prerequisite for topological control. The gas adsorption data show that permanent porosity is obtained even for interpenetrated structures. Overall, this contribution shows that when it is possible to control vertex geometry as illustrated herein for square paddlewheels, the task of controlling both the dimensionality and topology of the resulting structure becomes readily achievable by simply employing organic linkers of suitable geometry.

Acknowledgment. We are grateful to Prof. N. Jeong and Dr. K. S. Jeong for supplying the H_2*S*,*S*-DMEDBA link, Prof. H. K. Chae for synthesis of MOF-222, and Dr. J. L. C. Rowsell for his help in single-crystal X-ray structure collection and analysis of MOF-222. This work was supported by the U.S. Department of Energy (DE-FG36-05GO15001 and DE-FG02-08ER15935) and BASF (Ludwigshafen, Germany). J.K. thanks the Korea Research Foundation for Grant KRF 2003-070-C00029.

Supporting Information Available: Details of single-crystal X-ray structure collection and analysis for 5 MOPs and 11 MOFs including CIF files, ORTEPs, and tables of metrics. Powder X-ray diffraction patterns (simulated and experimental) and TGA traces. Ar isotherms and pore size distributions for MOF-601 and -602. This material is available free of charge via the Internet at http://pubs.acs.org.

JA803783C